"Roaming" Dynamics in CH_3CHO Photodissociation Revealed on a Global Potential Energy Surface†

Benjamin C. Shepler, Bastiaan J. Braams, and Joel M. Bowman*

Department of Chemistry and Cherry L. Emerson Center for Scientific Computation, Emory University, Atlanta, Georgia 30322

Received: March 17, 2008; Revised Manuscript Received: May 9, 2008

We present a quasiclassical trajectory study of the photodissociation of CH_3CHO to molecular and radical products, $CH_4 + CO$ and $CH_3 + HCO$, respectively, using global ab initio-based potentials energy surfaces. The molecular products have a well-defined potential barrier transition state (TS) but the dynamics exhibit strong deviations from the TS pathway to these products. The radical products are formed via a variational TS. Calculations are reported at total energies corresponding to photolysis wavelengths of 308, 282, 264, 248 and 233 nm. The results at 308 nm focus on a comparison with experiment [Houston, P. L.; Kable, S. H. *Proc. Natl. Acad. Sci. U.S.A.* **2006**, *103*, 16079] and the elucidation of the nature and extent of non-TS reaction dynamics to form the molecular products, $CH_4 + CO$. At the other wavelengths the focus is the branching ratio of these products and the radical products, $CH_3 + HCO$.

I. Introduction

Transition state theory (TST) is a cornerstone of reaction rate theory and it is taught in elementary texts in chemistry and biochemistry. The concept dates back to the 1930s[1,2] and its modern version with many improvements, including treatments of tunneling, variational effects, etc., has been reviewed in several excellent papers.[3–5]

The original, and largely intact version of the theory, applies to so-called activated reactions, that is reactions where the rate of reaction increases dramatically with temperature. For such reactions an energy barrier separating the reactants and products almost certainly must exist and this barrier is termed the transition state (TS). TST obtains the absolute value of the rate constant and its temperature dependence from the statistical/thermal properties of the TS, the reactants, and the products. It is this power and simplicity of the theory that are responsible for its widespread use. (Because the theory obtains the absolute value of the rate constant is it also referred to as "Absolute Rate Theory".)

Closely related to TST and now an inseparable extension of it is the concept of the Intrinsic Reaction Coordinate (IRC)[6,7] and its antecedent the reaction path.[8,9] The IRC is the minimum energy path in mass-weighted coordinates that smoothly connects reactants to products, with the TS being the first order saddle point at the highest energy along this path. Thus the IRC identifies a TS with a set of reactants and products and the potential energy on the IRC results in important dynamical extensions of TST, including various treatments of tunneling inclusion of "curvature effects", "corner-cutting", etc. These extensions of TST have been incorporated in very general and rigorous form in the Reaction Path Hamiltonian.[10]

Henceforth, TST will refer to TST with the associated IRC. It is important to stress that the information required to apply TST is the potential along the IRC and generally fairly small amplitude motion perpendicular to it. Thus, this is a very small "slice" of the full dimensional global potential energy surface (PES).

The concepts of TST are very much a part of modern treatments of reaction rates as illustrated in Figure 1, which depicts two IRCs connecting a single set of reactants to two sets of products via two different TS saddle points. This figure is based on the recent theoretical study of the reaction of $H + C_3H_8 \rightarrow H_2 + n\text{-}C_3H_7$, $H_2 + i\text{-}C_3H_7$ by Kerkeni and Clary.[11] As expected from this figure the rate constant for $n\text{-}C_3H_7$ is smaller than the one for $i\text{-}C_3H_7$ at temperatures where the average collision energy is comparable to the energy of the lower energy TS, in agreement with experiment. The lower panel in this figure is a cartoon depicting a rugged mountainous landscape including a path over a saddle point as well as another path that is quite different from the one over the saddle point. This cartoon is useful to keep in mind as we consider examples of non-TS/IRC dynamics in this paper. Also to avoid confusion we note at the outset that we purposely group TS and IRC dynamics together because this is the pervasive view of TST. A more general definition of the TS is a minimum flux, phase space dividing surface, depending on both coordinates and momenta, and not simply a TS with a coordinate definition, as is usually done in the literature, separating reactants and products.[3–5] It is an especially useful concept for reactions without a prominent saddle point and associated IRC. This is not the case for the $H_2CO \rightarrow H_2+CO$ and $CH_3CHO \rightarrow CH_4+CO$ reactions of interest here, which have well-defined prominent saddle point and IRC separating reactants from products.

The simplicity of TST mentioned above is clear if one considers the alternative approach, which is scattering theory (ideally quantum scattering; however, more often classical or quasiclassical scattering). In this approach much if not all of the PES is needed and clearly this alone is far more information and thus requires much more computational effort to obtain than what is needed to apply TST. Indeed in the work of Kerkeni and Clary a reduced dimensionality quantum approach was employed[12] in two degrees of freedom. The approach, which is

† Part of the "Stephen R. Leone Festschrift".

* To whom correspondence should be addressed. E-mail: jmbowma@emory.edu.

10.1021/jp802331t CCC: $40.75
Published on Web 07/03/2008

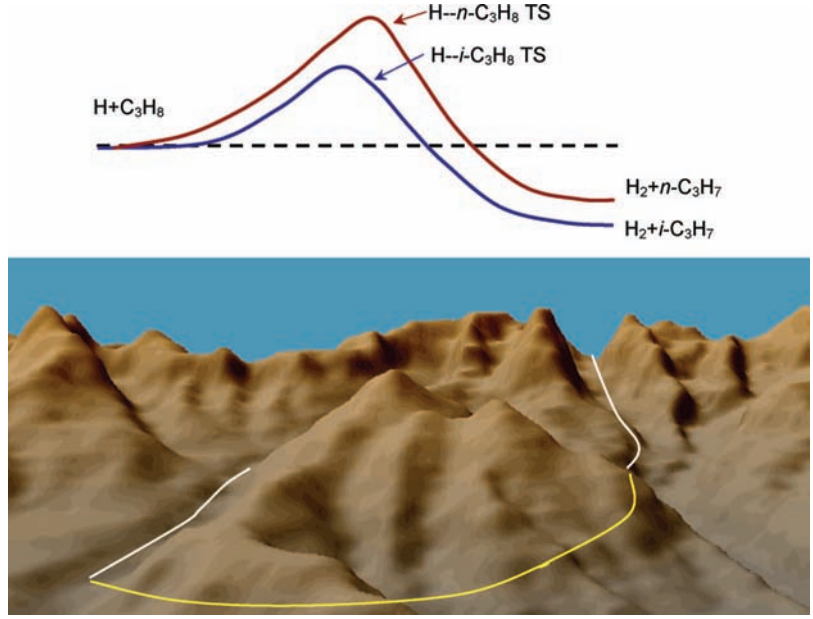

Figure 1. Schematic of two Intrinsic Reaction Coordinates and the potential on them describing the H + C_3H_8 reaction (upper panel) and a cartoon of a potential energy surface illustrating several pathways to proceed from an initial configuration ("reactants") to the same final configuration ("products").

built on the TST scaffold, that is considering each reaction independently, requires more computational effort than a simple TST calculation but far less than a full dimensional quantum one. The advantage of this reduced dimensionality approach is that it incorporates the dynamical effects of tunneling, curvature, and recrossing, albeit not exactly.

What can cause deviations from or even "failure" of TST (as defined above)? As the cartoon in the lower panel of Figure 1 is meant to suggest there may be more than one pathway connecting reactants and products, and not all paths have a saddle point TS. There are in the literature numerous examples of deviations and failures of TST and space does not permit an exhaustive review of these. Instead we give a sampling of notable examples and present a very recent and striking example in the photodissociation of CH_3CHO in the main body of this paper.

Deviations from TST have been discovered as a result of the application of scattering theory to the study of reaction dynamics since the 1960s. Most of the early scattering calculations were for triatomic systems. An early and striking example of non-TS dynamics was reported for the triatomic reaction H + ICl where the product HCl was formed with a bimodal distribution of internal ro-vibrational energies.[13,14] Two "microscopic mechanisms", "direct" and "migratory" were introduced to describe the reaction dynamics. The non-TS migratory mechanism was largely attributable to the very small barrier of this reaction (around 0.1 kcal/mol or less) compared to the thermal collision energies of the experiment. A recent and detailed study of the analogous H + FCl reaction, which shows these two mechanisms, was reported by Sayos et al.[15] using quasiclassical trajectory (QCT) calculations.

This failure of TST is not too surprising since at energies well above the TS there is less justification for the assumption that the dynamics will be governed by the IRC. Such deviations have been seen numerous times now in dynamical calculations and their consequences for experiment have been reported in a number of QCT and experimental studies for the H + HBr[16] and H + CH_4 reactions[17,18] employing translationally "hot" H atoms in the experiments. TST will also fail, or more precisely not apply, if there is not an obvious TS governing the reaction. This somewhat surprising situation was nicely exemplified perhaps first for the H_2 + CN → HCN + H reaction[19] and also the Cl + HCN → HCl + CN reaction using the H_2CN PES.[20] In these cases a TS pathway is present and is in fact dominant; however, there is a second pathway via the H_2CN complex, which does not have a saddle point barrier but a ridge that separates H_2 + CN and the H_2CN complex. In addition to this novel ridge feature, QCT calculations of the Cl + HCN reaction exhibited aspects of the two microscopic mechanisms noted above for the H + ICl reaction.

Another recent example of a reaction that proceeds via two pathways is H + HCO → H_2 + CO.[21] One pathway is via the deep H_2CO complex and the other is a direct, barrierless abstraction reaction. This reaction was studied with QCT calculations at a energy of 0.01 eV and using a global ab initio PES.[22] At this energy the product H_2 exhibited a striking bimodal vibrational state distribution with the major peak at $v = 7$, attributed to the abstraction pathway, and a smaller peak at $v = 1$ or 0, attributed to the complex-forming pathway. Additional QCT calculations of this reaction using the PES of ref 22 have focused on the importance of these two pathways in the prediction of low-pressure rate constants.[23]

Another example of a reaction without any obvious TS saddle point for an intermediate step is the reaction $O(^3P)$ + CH_3 → H + H_2 + CO[24] (one of six possible product channels). In this reaction no TS saddle point for the initial H_2 elimination from CH_3O^* could be located and so a "direct-dynamics" QCT calculation was undertaken. Based on 240 such trajectories no TS was located; however, H_2 + HCO products were formed which presumably went on to produce the final products above.

The $O(^3P)$ + CH_3 and H + HCO reactions are examples of a large class of chemical reactions that proceed primarily via a series of negative energy (relative to the energy of the reactants) complexes, which are typically separated by saddle points, again often but not always of negative energy. Other examples from our group are the $C(^3P, ^1D)$ + C_2H_2[25] and OH + NO_2[26] reactions that we have studied with global full dimensional PESs. Cation and anion-molecule reactions also exhibit the properties of the

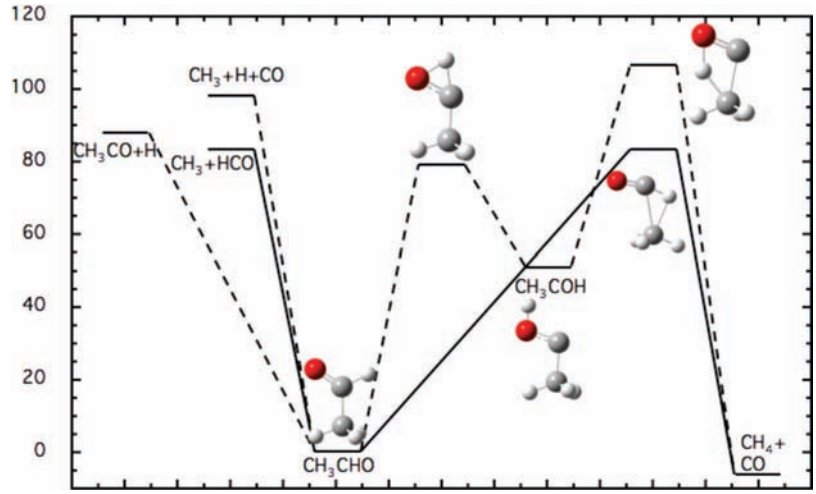

Figure 2. Schematic of benchmark energetics (given in Table 1) of some of the CH_3CHO stationary points and fragments and several structures.

complex-forming reactions. Extensive research employing direct-dynamics QCT calculations has found striking and significant non-IRC dynamics for a number of such reactions.[27,28]

Most of our research on non-TS dynamics has focused on QCT calculations of the photodissociation of H_2CO [29–35] and very recently on CH_3CHO.[36] The H_2CO research has benefited enormously from collaborations with experiment. The dissociation of H_2CO to the molecular products, $H_2 + CO$, has been done in collaboration with Arthur Suits and co-workers and dissociation to the radical products, $H + HCO$ has been done in collaboration with Scott Kable and co-workers. In the case of the molecular products a "roaming" non-TS mechanism was identified[29] as a significant secondary pathway to make $H_2 + CO$. However, the major pathway to these products is via the well-known saddle point TS. In brief the roaming path originates in the incipient H−HCO product channel where these fragments do not have sufficient energy to dissociate but instead orbit each other (visiting the high energy cis and trans hydroxycarbene isomers of H_2CO) and then "self-react" to form $H_2 + CO$. (Animations of several of these roaming trajectories can be found at http://www.chemistry.emory.edu/faculty/bowman/H2CO.htm.) One signature of this roaming pathway is very highly vibrationally excited H_2; H_2 formed from the conventional TS pathway is vibrationally cold. (The bimodal H_2 vibrational distribution in the H_2CO dissociation is closely related to the bimodal distribution mentioned above for the H+HCO reaction.)

It is important to stress that the QCT studies surveyed above all require the input of the molecular potential. Those using direct-dynamics generally are limited to several hundred trajectories and propagation times less than 1 ps because the ab initio evaluation of the potential and its gradient at each time step is very computer intensive. The advantage and great appeal of the approach is that it eliminates the need to have an analytical expression for the PES. However, having an expression for the PES is ideal, since it permits running many thousands of trajectories for 10 ps or longer. We have taken this approach and will describe the methods we use in the application to CH_3CHO photodissociation.

To conclude this Introduction we note that a review of multiple pathways in reactions is due to appear.[37] We also wish to note the role of prereactive wells that can strongly influence chemical reactivity. Some important examples include the influence of a van der Waals well in determining the branching ratio of the HCl and DCl products in the Cl + HD reaction and the sizable error made by TST in predicting this ratio.[38] Another example is the enhancement of low-energy reactivity in the $O(^3P) + HCl$[39] and $F + H_2$[40] reactions due to resonances in van der Waals wells.

In the next section we present results of calculations of CH_3CHO photodissociation and contrast the results with the simpler but closely related H_2CO photodissociation. A key element of this work is the development of a global PES and we briefly explain our approach to obtain this PES for CH_3CHO.

II. CH_3CHO Photodissociation

The first joint theoretical experimental study of the photodissociation dynamics of CH_3CHO to form the molecular products CH_4+CO was reported in 2001 by Gherman et al.[41] The experiment was done at 248 nm and the ro-vibrational energy of the CO product was measured. No vibrationally excited CO was detected and the rotational energy distribution was fit to a Boltzmann distribution with a temperature of 1300 ± 90 K. Calculations done with density functional theory/B3LYP were able to locate and characterize the TS for the molecular channel; the barrier height was reported to be 85.3 kcal/mol. In fact, two first order saddle points were located differing by only 5.4 kcal/mol and the lower energy one, which also had a "CO-like" normal mode was selected as the relevant TS (the IRC was not reported). Based on the geometry of the preferred TS it was argued that the CO should be vibrationally "cold" and rotationally "hot".

Subsequently Kurosaki and Yokoyama[42] reported a direct-dynamics QCT calculation of this photodissociation (at 248 nm) by doing roughly 100 trajectories initiated at the molecular saddle point TS (the one identified by Gherman et al.) and in the "direction" of dissociation. Later calculations were done with roughly 700 trajectories.[43] These calculations are analogous to previous QCT calculations of the H_2CO photodissociation, which were initiated at the $H_2 + CO$ molecular saddle point.[44–46] (It is interesting, in view of the theme of this paper, to note the role of the TS in many QCT calculations with H_2CO and CH_3CHO being two examples. The great advantage of the combined TS-QCT approach is that the trajectories are relatively short and thus are feasible with the costly direct-dynamics approach.) The resulting CO rotational distribution from the most recent calculations[43] is quite hot and fairly symmetric about a peak value at roughly $j_{CO} = 58$. No direct comparison was

TABLE 1: Comparison of the Fitted Potential Energy Surfaces and Ab Initio Benchmark Calculations for Selected Stationary Points on the H_4C_2O Surface (kcal/mol)[a]

species	CCSD(T)/ CBS+CV	fifth order PES	sixth order PES
1. acetaldehyde	0.0	0.0	0.0
2. vinyl alcohol	9.1	13.5	15.0
3. hydroxyethylidene	50.8	54.0	53.4
4. TS1 (1−2)	70.8	72.4	72.5
5. TS2 (1−3)	83.0	87.2	85.6
6. TS3 (2−3)	75.5	87.6	81.6
7. TS4 (1−10)	87.5	84.8	96.1
8. TS5 (3−10)	110.9	102.6	108.0
9. TS6 (1−11)	86.0	91.8	95.1
10. $CH_4 + CO$	−2.0	−2.5	−1.6
11. $CH_2CO + H_2$	35.2	43.5	37.1
12. $CH_3 + HCO$	90.8	91.0	94.0
13. $CH_3CO + H$	95.6	100.9	100.5
14. $CH_2CHO + H$	102.5	103.7	103.9
15. $CH_3 + CO + H$	110.5	104.7	106.0
16. $CH_2CH + OH$	124.5	141.7	142.0

[a] The notation TS$k(n-m)$ refers to the TS between species n and m and k is an ordering label.

made with experiment of Gherman et al., perhaps because the interpretation of experiment at 248 nm is complicated by the possibility that another source of CO is the energetically open three-body channel, $CH_3 + H + CO$.

Subsequent to the Kurosaki and Yokoyama papers Kable and Houston reported an experimental determination of the CO rotational distribution at 308 nm (where the three body channel is closed) as well as data on the $\mathbf{V} \perp \mathbf{j}_{CO}$ vector correlation[47] where $\mathbf{V}$ is the fragment relative velocity vector. Their interpretation of the data led them to label this photodissociation a "second example of roaming" (the first example cited in their paper was the roaming mechanism in H_2CO photodissociation.) Stimulated by this work we developed a global PES for the CH_3CHO dissociation and reported this briefly in a preliminary account along with results of some QCT trajectory calculations.[36] We did report evidence of a roaming mechanism for the $CH_4 + CO$ products. Next we describe the development of the PES and present new benchmark ab initio calculations of the energies of a number of relevant stationary points and fragments.

A. Potential Energy Surface. The complete, global PES for CH_3CHO is quite complex. One measure of the complexity can be gained by inspection of Figure 1 of a recent paper by Yang et al.[48] which shows 98 stationary points obtained from DFT (B3LYP/6−311++G(d,p)) and CCSD(T)/cc-pVTZ//B3LYP/6−311++G(d,p) calculations. An indication of this complexity was already clear in the early computational work of Gherman et al., which located three possible saddle points for the $CH_4 + CO$ channel. An energy schematic of the stationary points and fragments relevant to our dynamics calculations is given in Figure 2. The energies in this figure were obtained using new benchmark calculations described below.

Due to the complexity of this potential the fits we did were not able to achieve the level of precision obtained for other systems. For example, for H_2CO the PES has "only" three saddle points, three minima, and two reaction channels. The PES developed for H_2CO[22] reproduces these saddle point energies, which are 80−86 kcal/mol above the global minimum, to within 1−3 kcal/mol. In view of the lack of this level of precision for CH_3CHO we fit two global PESs to the ab initio energies as described next.

Each PES is a fit to roughly 150 000 ab initio energies, computed with the coupled cluster singles and doubles method with a perturbative treatment of triple excitations [RCCSD(T)],[49] as implemented in the MOLPRO suite of codes.[50] Several different basis sets were used: the Dunning correlation consistent polarized valence double and triple-ζ basis set (cc-pVDZ) and (cc-pVTZ)[51] and the augmented cc-pVTZ (aug-cc-pVTZ) basis set.[52] At the acetaldehyde global minimum the aug-cc-pVTZ energy is below the cc-pVDZ and cc-pVTZ energy and all calculated cc-pVDZ and cc-pVTZ energies were shifted by their respective differences with the aug-cc-pVTZ energy before fitting the combined data set. This data set consisted of electronic energies for the complex regions and fragments for all possible reaction channels. There are three principal isomers of H_4C_2O: acetaldehyde (CH_3CHO), hydroxyethylidene (CH_3COH), and vinyl alcohol (CH_2CHOH). For simplicity we indicate only the first two in Figure 2. We sampled all three isomers and their transition regions mainly by running classical dynamics calculations using preliminary PESs. These calculations were run at multiple total energies from about 10 to 190 kcal/mol relative to a local minimum, in order to sample well the vicinity of the local minimum and also to describe much larger amplitude motion but terminating trajectories whenever dissociation occurred. Initial geometries were at minima and also saddle points. Further geometries for the database in the complex region were obtained by applying random displacements directly to local minima and stationary points on a preliminary fitted surface. For reasons of computational cost most calculations in the complex were calculated with the cc-pVDZ basis, and about 99 000 configurations were obtained that way and roughly 700 geometries were calculated using the aug-cc-pVTZ basis.

In order to describe dissociation to fragments the database was supplemented with energies of numerous fragment channels. This was done by separating the fragments by roughly 100 bohr and assigning the energy as the sum of the fragment energies. For the cases where the fragments contain one or two C and or O atoms we employed the aug-cc-pVTZ basis. (The fragment geometries were sampled in a similar manner as discussed for the H_4C_2O complex, and indeed these data and associated surfaces are of interest in their own right and are used in other surfaces.) Cases where each fragment has an odd number of electrons are of special interest, because a direct ab initio calculation of the fragmentation to these open shell fragments cannot be done reliably using the single reference RCCSD(T) method. Thus the PES effectively interpolates through these problematic regions by using isolated fragment energies. (This interpolation was shown previously[36] to be quite realistic by comparing the PES against direct MRCI+Q calculations.) For fragmentation to closed shell species energies were obtained over the entire range of fragmentation.

Energies from the following fragment channels, in order of relevance to the dynamics calculations described below were included in the database: $CH_4 + CO$, $CH_3 + HCO$, $CH_3 + H + CO$, $CH_3CO + H$, *$CH_2CO + H_2$*, *$C_2H_2 + H_2O$*, *$H_2CO + {}^1CH_2$*, plus several other very high energy channels. The channels in italics are not observed in any significant amount in the photodissociation dynamics calculations described in the following subsection. Roughly 50 000 energies from these channels were included in the final database of energies of roughly 150 000 for the fits.

Two fits to these data were done. In general our fits use a basis of polynomials in Morse-like variables in all the internuclear distances. The polynomials have the important property of being invariant with respect to all permutations of like atoms and details can be found elsewhere.[18,25,26] For CH_3CHO there are 48 such permutations. The fits differ in the total order of

the polynomial basis; one PES is a fifth order fit and the other is a sixth order fit. The fifth order fit is roughly half as CPU-intensive to evaluate as the sixth order fit. However, because neither fit is highly precise (see Table 1) we have used both in the dynamics calculations as a way to check the robustness of the results.

We have performed benchmark calculations based on a coupled cluster composite approach.[53] For this work, the first step in the composite approach was to optimize the geometries using CCSD(T) with the aug-cc-pVTZ basis sets. At these optimized geometries single point CCSD(T) calculations were carried out with the cc-pV*n*Z (n = T, Q, 5) basis sets and the energies were extrapolated to the complete basis set (CBS) limit. A core-valence (CV) correction was then calculated as the difference in energy between all-electrons correlated and valence-only electrons correlated calculations with the CCSD(T) method and employing the aug-cc-pwCVTZ[54] basis sets. The energies for various stationary points and fragments that are relevant to the dynamics calculations are given in Table 1 along with the corresponding ones for the fifth and sixth order PESs. As seen, both PESs are in reasonable agreement with benchmark energies, and this is especially gratifying considering the that PESs are fits to energies from lower level ab initio calculations. Note that the fifth order PES energy for TS4, the TS for connecting CH_3CHO to CH_4 + CO is only 2.7 kcal/mol below the benchmark value whereas the sixth order PES is almost 10 kcal/mol higher. For other saddle points and fragment energies the sixth order PES is more accurate than the fifth order PES.

B. Dynamics Calculations. QCT calculations were performed primarily to address the photodissociation experiment of Houston and Kable at 308 nm, specifically the CO rovibrational distributions. The calculations were carried out on both PESs starting at the CH_3CHO equilibrium global minimum with total energy of 127.6 kcal/mol, which is the sum of the (harmonic) CH_3CHO zero-point energy plus the energy of a 308 nm photon. Also, the total angular momentum was fixed at zero. We refer to these as "EQ" trajectories and roughly 7600 and 4200 of them were run on the fifth and sixth order PES, respectively. Of these, 1784 and 777, respectively, resulted in CH_4 + CO products. The remainder gave CH_3 + HCO and CH_3 + H + CO products. However, all of the triple fragment products violate the zero-point energy (ZPE) constraint, i.e., they are all formed with less than ZPE as they must since this channel is energetically (with ZPE) closed. Also a large number of trajectories giving the energetically open radical products also violate ZPE constraints. We will discuss this is in more detail below.

An additional 5000 trajectories were run on the fifth order PES to simulate excitation at wavelengths of 282, 264, 248 and 233 nm to investigate the branching between the molecular and radical channels, CH_4 + CO and CH_3 + HCO, respectively.

CH_4 + CO. Most of the CO formed from the EQ dynamics is in the ground vibrational state, in accord with the experiment of Gherman et al. and Houston and Kable. Thus we focus on the CO rotational distribution of CO in this vibrational state. An important aim of these calculations is to determine the extent of TS vs non-TS dynamics. To do this we also performed direct-dynamics QCT calculations initiated at the molecular saddle point, TS4, at the MP2/cc-pVDZ level of theory and basis. These are denoted "TS DD" and by definition these represent the TS dynamics. These calculations are virtually identical in method and level of ab initio theory and basis to those reported at 248 nm by Kurosaki.[42,43] The results of these calculations and the comparison with experiment are shown in Figure 3. To simplify

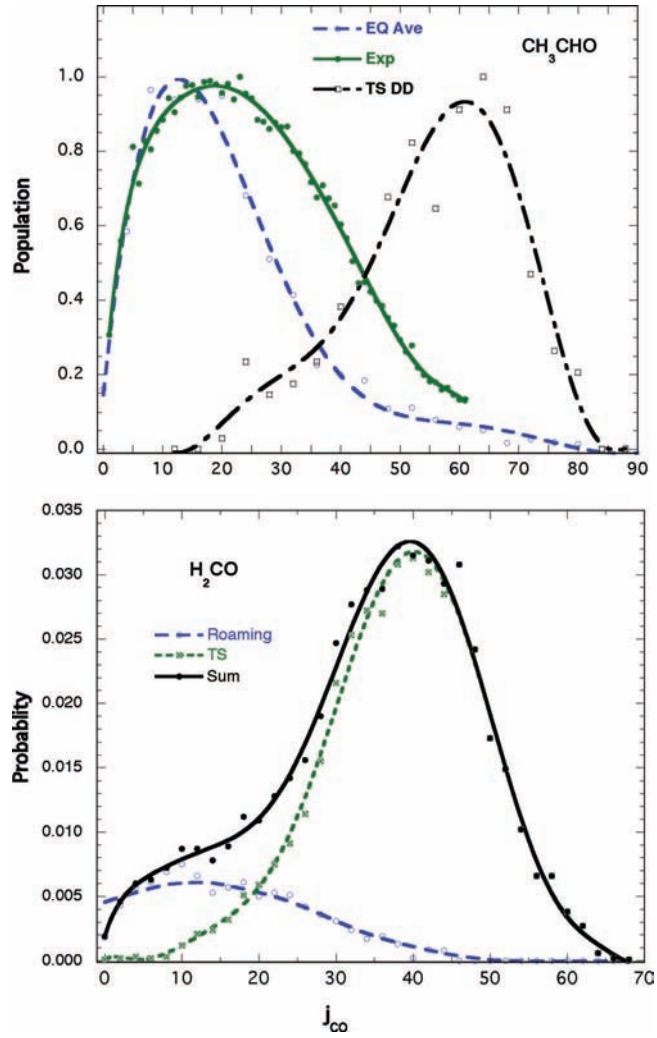

Figure 3. CO rotational distribution for CH_3CHO (upper panel) and H_2CO (lower panel). See text for an explanation of the curves.

the plot we give the average of the EQ distributions obtained on the fifth and sixth order PESs. For reference we have also plotted in the lower panel of this figure the previously calculated CO(v = 0) rotational distribution from EQ trajectories for H_2CO photodissociation run at roughly the same total photolysis energy[30] on the global PES and initiated at the H_2CO global minimum. This distribution for H_2CO was carefully deconstructed, as shown, into TS and non-TS components. The TS component agrees virtually exactly with the results of dynamics initiated at the H_2+CO molecular TS of the same PES[21] and also with earlier QCT calculations initiated at the molecular saddle point.[44–46] The roaming dynamics of the H_2CO dissociation has been illustrated in the literature already[29,32,33] in the form of trajectory snapshots and trajectory animations (mentioned in the Introduction). Here we show another representation of this dynamics in Figure 4, where the time evolution of the two CH bond lengths is shown along with the variation in the potential energy (measured relative to the H_2CO equilibrium geometry). The early history of the trajectory where one H atom is vibrating with large amplitude against the HCO core is not shown. As seen between time steps 2000 and 3000 one CH distance is executing large amplitude oscillatory motion. This is the motion of an H atom oscillating relative to the HCO fragment along a CH bond. Then between 3000 and 4000 the motion changes qualitatively. After reaching a large separation the H atom maintains a large CH distance of roughly 7 bohr.

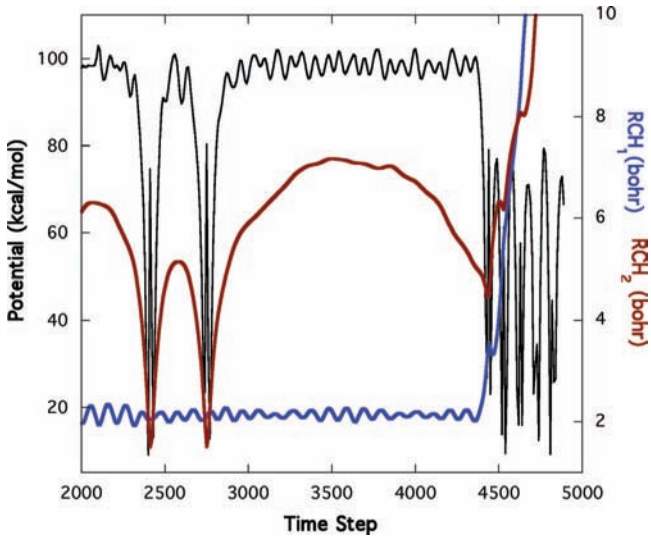

Figure 4. Time dependence of the two CH distances and the potential for an H_2CO roaming trajectory that results in CO + H_2, with H_2 vibrationally excited. One time step in this figure is roughly 0.1 fs.

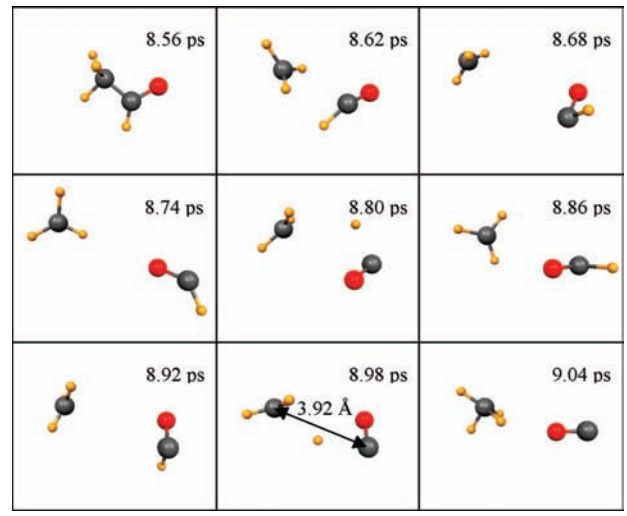

Figure 5. "Snapshots" of a roaming trajectory for CH_3CHO dissociation to form CH_4 and CO products.

This is where it and the HCO fragment are mutually "roaming" around each other. During the roaming the H atom is "visiting" the regions of the high-energy cis and trans hydroxycarbene isomers of H_2CO. The small oscillations in the potential in this time window are due mainly to the relatively small amplitude oscillatory motion of HCO. Finally, owing to this orientation between the H and HCO, abstraction of the H atom from HCO can and does take place at a large HH separation and the product H_2 is formed vibrationally very hot (the CO is vibrationally and rotationally cold). The large variation in the potential at the end of the trajectory is mainly due to the large amplitude H_2 vibration.

Returning now to Figure 3, we see that for H_2CO the non-TS, roaming, component of the total rotational distribution, while significant, is smaller than the TS component, and appears as a "bump" in the rotational distribution at low j_{CO}. The major portion of the distribution, which is obtained from TS dynamics, agrees well with the first experiments of Moore and co-workers,[55] which were done at a photolysis energy which did not show a bump at low j_{CO}. This feature was seen in the later, important higher energy experiment of van Zee and Moore,[56] who clearly understood that it was significant and possibly a signature of non-TS dynamics. This situation is clearly reversed for CH_3CHO, where experiment is in substantial disagreement with the TS DD rotational distribution but is in good agreement with the EQ calculations. The experimental distribution is broader than the EQ ones and this might be due in part to the fixed value of the CH_3CHO angular momentum of zero in the calculations. However, some of the difference may also be due to inaccuracies in the PESs. This slight difference notwithstanding we conclude that the extent of non-TS dynamics in CH_3CHO is much greater than in the case of H_2CO.

To investigate the nature of the non-TS dynamics we have examined a number of non-TS trajectories for CH_3CHO and do find incipient CH_3-HCO fragmentation, as speculated by Houston and Kable, in analogy with the incipient radical fragmentation in H_2CO. There are a number of ways to do this investigation and in our preliminary report[36] we did an analysis of the C−C distance when the H atom transfer occurs to form CH_4 + CO as a function of j_{CO}. We found that for j_{CO} less than 45 the average C−C distance is 3.8 Å with a standard deviation of 0.7 Å, and for j_{CO} greater than 45 this average distance is 2.3 Å. Note that at the molecular TS saddle point the C−C distance is 2.1 Å. Thus, the conclusion based on our equilibrium trajectories is that for the majority of dissociation events (where j_{CO} is less than 45) in the critical geometry where the CH_4 + CO are formed the C−C bond distance is significantly larger than the value at the conventional saddle point. In Figure 5 we give nine frames of a trajectory where the H atom transfer occurs at a large C−C distance. As seen in the earlier time history a near separation of CH_3CHO into the CH_3 and HCO fragments is followed by by transfer of the H from HCO to CH_3 at large C−C separation. It is interesting to note the semiquantitative agreement between the average value of the C−C bond length for the non-TS pathway to the molecular products and the value reported recently by Harding et al. [56] of 3.4 Å for a very floppy roaming TS.

CH_3 + HCO. We now consider the radical products. As noted by Gherman et al.[41] the radical fragments CH_3 + HCO correlate with both T_1 and S_0 and they reasoned that they are formed dominantly from T_1 especially at lower photolysis energies. They argued that at higher photolysis energies relaxation of S_1 CH_3CHO to S_0 dominates over T_1 and they concluded that "At the experimentally convenient wavelength of 248.4 nm (42 560 cm^{-1}) the CO + CH_4 channel is the dominant channel". They did not do a direct measurement of the branching between the molecular and radical products.

We have calculated the molecular and radical channel branching using the fifth order PES (which is for S_0) as a function of energy. First note that the total energy of the EQ trajectories corresponding to 308 nm excitation exceeds the energetic threshold for formation of the radicals in their ground ro-vibrational state by 10 kcal/mol. In the harmonic approximation the combined ZPE of the products is roughly 27 kcal/mol and thus the total energy is 37 kcal/mol above the classical energetic threshold for these products. This large disparity between the classical threshold and the (correct) quantum threshold leads us to expect serious issues with violation of ZPE in the trajectory calculations and indeed, as already noted, we see this. (A full-dimensional quantum treatment of the dynamics would of course not suffer from this violation; however, at present and even in the foreseeable future such a calculation is not feasible.) The analogous situation was observed for H_2CO dissociation to HCO + H[30] and in that case we imposed the usual constraint of discarding trajectories that yield HCO with less than ZPE. This guarantees that the branching ratio to this

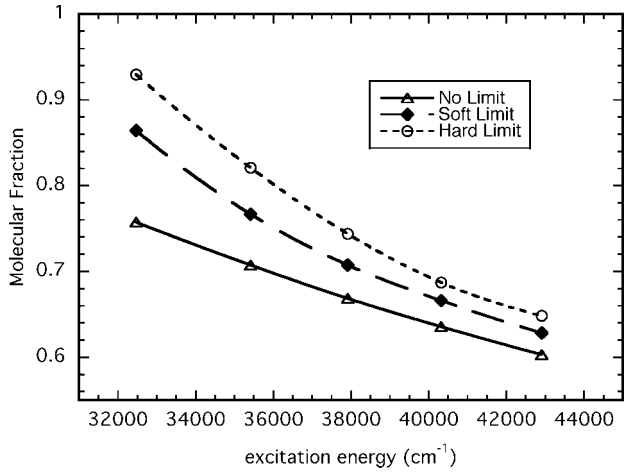

Figure 6. Branching ratio of the $CH_4 + CO$ products to the sum of these products plus the $CH_3 + HCO$ products as a function of the excitation energy. The energy range corresponds to a photolysis wavelength range of 308−233 nm.

channel is zero at energies below the correct energetic threshold. In the present case, where the radicals are both molecular, the energetic threshold can be enforced by what we term "hard" or "soft" limits. The former is where we require each product to have at least ZPE and the latter is where we require the sum of the vibrational energes to be at least the total ZPE. When imposing the hard limit 85% of the $CH_3 + HCO$ products are discarded at the lowest excitation energy and this steadily decreases to roughly 40% of the products being discarded at the highest excitation energy we consider. In contrast, roughly one-third of the $CH_4 + CO$ products are discarded (mostly due to ZPE violation in CO) at all energies when using the hard limit (although the number decreases slightly with excitation wavelength). In the case of the soft limit, 50−10% of the radical trajectories are discarded as the excitation energy is increased over the range considered. Virtually no molecular trajectories are discarded in the soft limit owing to the large vibrational excitation in CH_4.

Using these two limits we have calculated the ratio of the molecular products to the sum of molecular plus radical products as a function of photolysis energy and plot the results in Figure 6. For reference we also give the ratio with no constraint on the vibrational energy of the products. As seen with either the hard or soft limit the branching ratio starts at roughly 0.9 at 32 467 cm^{-1} (corresponding to 308 nm) and decreases slowly to roughly 0.65 at 43 000 cm^{-1}. Note at 40 323 cm^{-1}, which corresponds to 248 nm, the ratio is roughly 0.7. Thus the ratio of the molecular channel to the radical channel is roughly 2.5:1. This does indicate a substantial preference for the molecular channel at 248 nm in rough accord with the statement quoted from Gherman et al.; however, the present results are obtained only considering S_0 and so perhaps the accord is somewhat coincidental.

It is interesting that the radical channel is relatively less probable than the molecular one even up to total energies roughly 41 kcal/mol above the radical energetic threshold. By contrast in H_2CO the radical and molecular channels are calculated to be equally probable at a total energy only 2.8 kcal/mol above the radical energetic threshold.[30] This large difference between H_2CO and CH_3CHO may be correlated with the large difference in the extent of non-TS dynamics in the two cases. In both cases the non-TS roaming pathway to molecular products occurs in the incipient radical and thus this pathway competes with the radical channel. Thus in CH_3CHO where evidently the non-TS roaming is dominant, in contrast to H_2CO (cf. Figure 3), it is clear that most of the CH_3CHO dissociation flux is directed by the PES to this region and the dominant non-TS dynamics "shuts off" the radical channel to a large degree. It is interesting that a recent experimental paper investigating CH_3CHO photodissociation at 248 nm reports no CH_3.[58] It is interesting to speculate that the relatively minor production of $CH_3 + HCO$ (on S_0) is a consequence of the dominant non-TS dynamics.

We conclude this section by noting and commenting on the other energetically accessible products that we do not see in any significant amount in the QCT calculations. These are $CH_2CO + H_2$, $C_2H_2 + H_2O$ and $CH_2CHO + H$, which together make up $\ll$1% of the products observed in our calculations. Chief among these may be $CH_2CO + H_2$, which has a TS from CH_3CHO that is nearly isoenergetic to the TS for formation of $CH_4 + CO$. At this time it is uncertain why more of this product is not observed. One possibility is that because most of the flux of CH_3CHO dissociation is in the region of the CH_3-HCO channel there is no simple, obvious alternate roaming pathway to make $CH_2CO + H_2$. This clearly warrants future investigation.

Summary

We presented a theoretical/computational study of the photodissociation of CH_3CHO on the ground electronic state. This was done using global potential energy surfaces fit to roughly 150 000 ab initio electronic energies and quasiclassical trajectories initiated at the CH_3CHO equilibrium configuration and also using direct-dynamics initiated at the saddle point transition state for the molecular channel, $CH_4 + CO$. Comparisons of the CO rotational distributions obtained with these two sets of QCT calculations and those from a recent photodissociation experiment done at 308 nm indicate substantial non-transition state dynamics for this channel. The nature of the non-TS dynamics was elucidated by consideration of a representative "roaming" trajectory which indicates that the molecular products are formed in the regions of nearly separated radical fragments, $CH_3 + HCO$. Additional QCT calculations were done at higher energies to determine the branching between the molecular channel and the radical channel $CH_3 + HCO$.

Acknowledgment. B.C.S. thanks the National Science Foundation (CHE-0625237), B.J.B. thanks the Office of Naval Research (N00014-05-1-0460), and J.M.B. thanks the Department of Energy (DE-FG02-97ER14782) for financial support. J.M.B. thanks Professor Dudley Herschbach for discussions about non-TS dynamics and alerting him to ref 14. J.M.B. also thanks David Osborn for a preprint of ref 37.

References and Notes

(1) Eyring, H. *J. Chem. Phys.* **1935**, *3*, 107.
(2) Pelzer, H.; Wigner, E. *Z. Phys. Chem. Abt. B* **1932**, *15*, 445.
(3) Pechukas, P. *Annu. Rev. Phys. Chem.* **1981**, *32*, 159.
(4) Truhlar, D. G.; Garrett, B. C.; Klippenstein, S. J. *J. Phys. Chem.* **1996**, *100*, 12771.
(5) Garrett, B. C.; Truhlar, D. G. In *Theory and Applications of Computational Chemistry, The First 40 Years*; Dykstra, C, Frenking, G, Kim, K. S., Scuseria, G. E. Eds.; Elsevier: Amsterdam, 2005; Chapter 5.
(6) Fukui, K. *J. Phys. Chem.* **1970**, *74*, 4161.
(7) Ishida, K.; Morokuma, K.; Komornicki, A. *J. Chem. Phys.* **1977**, *66*, 2153.
(8) Hofacker, L. *Z. Naturforsch. Tei1.4* **1963**, *18*, 607.
(9) Marcus, R. A. *J. Chem. Phys.* **1965**, *43*, 1598.
(10) Miller, W. H.; Handy, N. C.; Adams, J. E. *J. Chem. Phys.* **1980**, *72*, 99.
(11) Kerkeni, B.; Clary, D. C. *Phys. Chem. Chem. Phys.* **2006**, *8*, 917.

(12) Bowman, J. M. *Adv. Chem. Phys.* **1985**, *61*, 115.
(13) Nazar, M. A.; Polanyi, J. C.; Skrlac, W. J. *Chem. Phys. Lett.* **1974**, *29*, 473.
(14) Polanyi, J. C. in *The Chemical Bond*; Zewail, A. Ed.; Academic, San Diego, 1992; Chapter 7.
(15) Sayós, R.; Hernando, J.; Francia, R.; González, M. *Phys. Chem. Chem. Phys.* **2000**, *2*, 523.
(16) Pomerantz, A. E.; Camden, J. P.; Chiou, A. S.; Ausfelder, F.; Chawla, N.; Hase, W. L.; Zare, R. N. *J. Am. Chem. Soc.* **2005**, *127*, 16368.
(17) Camden, J. P.; Bechtel, H. A.; Ankeny-Brown, D. J.; Martin, M. R.; Zare, R. N.; Hu, W.; Lendvay, G.; Troya, D.; Schatz, G. C. *J. Am. Chem. Soc.* **2005**, *127*, 11898.
(18) Xie, Z.; Bowman, J. M. *Chem. Phys. Lett.* **2006**, *429*, 355.
(19) ter Horst., M.; Schatz, G. C.; Harding, L. B. *J. Chem. Phys.* **1996**, *105*, 558.
(20) Troya, D.; Gonzalez, M.; Wu, G.; Schatz, G. C. *J. Phys. Chem.* **2001**, *105*, 2285.
(21) Rheinecker, J.; Zhang, X.; Bowman, J. M. *Mol. Phys.* **2005**, *103*, 1067.
(22) Zhang, X.; Zou, S.; Harding, L. B.; Bowman, J. M. *J. Phys. Chem. A* **2004**, *108*, 8980.
(23) Troe, J.; Ushakov, V. *J. Phys. Chem. A* **2007**, *111*, 6610.
(24) Marcy, T. P.; Dıaz, R. R.; Heard, D.; Leone, S. R.; Harding, L. B.; Klippenstein, S. J. *J. Phys. Chem. A* **2001**, *105*, 8361.
(25) Park, W. K.; Park, J.; Park, S. C.; Braams, B. J.; Chen, C.; Bowman, J. M. *J. Chem. Phys.* **2006**, *125*, 081101.
(26) Chen, C.; Schepler, B. C.; Braams, B. J.; Bowman, J. M. *J. Chem. Phys.* **2007**, *127*, 104310.
(27) Sun, L. P.; Song, K. Y.; Hase, W. L. *Science* **2002**, *296*, 875.
(28) López, J. G.; Vayner, G.; Lourderaj, U.; Addepalli, S. V.; Kato, S.; deJong, W. A.; Windus, T. L.; Hase, W. L. *J. Am. Chem. Soc.* **2007**, *129*, 9976.
(29) Townsend, D.; Lahankar, S. A.; Lee, S. K.; Chambreau, D.; Suits, A. G.; Zhang, X.; Rheinecker, J.; Harding, L. B.; Bowman, J. M. *Science* **2004**, *306*, 1158.
(30) Zhang, X.; Rheinecker, J. L.; Bowman, J. M. *J. Chem. Phys.* **2005**, *122*, 114313.
(31) Bowman, J. M.; Zhang, X. *Phys. Chem. Chem. Phys.* **2006**, *8*, 321.
(32) Lahankar, S. A.; Chambreau, S. D.; Townsend, D.; Suits, F.; Farnum, J.; Zhang, X.; Bowman, J. M.; Suits, A. G. *J. Chem. Phys.* **2006**, *125*, 044303.
(33) Lahankar, S. A.; Chambreau, S. D.; Zhang, X.; Bowman, J. M.; Suits, A. G. *J. Chem. Phys.* **2007**, *126*, 044314.
(34) Farnum, J.; Zhang, X.; Bowman, J. M. *J. Chem. Phys.* **2007**, *126*, 134305.
(35) Yin, H. M.; Kable, S. H.; Zhang, X.; Bowman, J. M. *Science* **2006**, *311*, 1443.
(36) Shepler, B. C.; Braams, B. J.; Bowman, J. M. *J. Phys. Chem. A* **2007**, *111*, 8282.
(37) Osborn, D. L. Exploring Multiple Reaction Paths to a Single Product Channel. *Adv. Chem. Phys.* In press.
(38) Skouteris, D.; Manolopoulos, D. E.; Bian, W.; Werner, H-J.; Lai, L-H.; Liu, K. *Science* **1999**, *286*, 1713.
(39) Xie, T.; Wang, D.; Bowman, J. M.; Manolopoulos, D. E. *J. Chem. Phys.* **2002**, *116*, 7461.
(40) Balakrishnan, N.; Dalgarno, A. *Chem. Phys. Lett.* **2001**, *341*, 652.
(41) Gherman, B. F.; Friesner, R. A.; Wong, T-H.; Min, Z.; Bersohn, R. *J. Chem. Phys.* **2001**, *114*, 6128.
(42) Kurosaki, Y.; Yokoyama, K.;. *J. Phys. Chem. A* **2002**, *106*, 11415.
(43) Kurosaki, Y. *Chem. Phys. Lett.* **2006**, *421*, 549.
(44) Chang, Y-T.; Minichino, C.; Miller, W. H. *J. Chem. Phys.* **1992**, *96*, 4341.
(45) Chen, W.; Hase, W. L.; Schlegel, H. B. *Chem. Phys. Lett.* **1994**, *228*, 436.
(46) Peslherbe, G. H.; Hase, W. L. *J. Chem. Phys.* **2000**, *104*, 7882.
(47) Li, X.; Millam, J. M.; Schlegel, H. B. *J. Chem. Phys.* **2000**, *113*, 10062.
(48) Houston, P. L.; Kable, S. H. *Proc. Natl. Acad. Sci. U.S.A.* **2006**, *103*, 16079.
(49) Yang, X.; Maeda, S.; Ohno, K. *J. Phys. Chem. A* **2007**, *111*, 5099.
(50) Knowles, P. J.; Hampel, C.; Werner, H-J. *J. Chem. Phys.* **1993**, *99*, 5219 Erratum, J. Chem. Phys. 2000, 112, 3106.
(51) MOLPRO, version 2006.1, a package of ab initio programs, Werner, H-J.; Knowles, P. J.; Lindh, R.; Manby, F. R.; Schuetz, M.; Celani, P.; Korona, T.; Rauhut, G.; Amos, R. D.; Bernhardsson, A.; et al. see http,// www.molpro.net.
(52) Dunning, T. H., Jr. *J. Chem. Phys.* **1989**, *90*, 1007.
(53) Kendall, R. A.; Dunning, T. H., Jr.; Harrison, R. J. *J. Chem. Phys.* **1992**, *96*, 6796.
(54) Dixon, D. A.; de Jong, W. A.; Peterson, K. A.; Christe, K. O.; Schrobilgen, G. J. *J. Am. Chem. Soc.* **2005**, *127*, 8627.
(55) Peterson, K. A.; Dunning, T. H., Jr. *J. Chem. Phys.* **2002**, *117*, 10548.
(56) Ho. P.; Bamford, D. J.; Buss, R. J.; Lee, Y. T.; Moore, C. B. *J. Chem. Phys.* **1982**, *76*, 3630.
(57) van Zee, R. D.; Foltz, M. F.; Moore, C. B. *J. Chem. Phys.* **1993**, *99*, 1664.
(58) Harding, L. B.; Klippenstein, S. J.; Jasper, A. W. *Phys. Chem. Chem. Phys.* **2007**, *9*, 4055.
(59) Rubio-Lago, L.; Amaral, G. A.; Arregui, A.; Izquierdo, J. G.; Wang, F.; Zaouris, D.; Kistopoulos, T. N.; Bañares, L. *Phys. Chem. Chem. Phys.* **2007**, *9*, 6123.

JP802331T